

## Article

# Interactions of Acetylene-Derived Thioester Collectors with Gold Surfaces: A First-Principles Study

Xianyang Qiu <sup>1,2,3</sup>, Yuechao Qi <sup>1,\*</sup>, Dezhou Wei <sup>1</sup>, Faming Zhang <sup>2,3</sup> and Chenghang Wang <sup>2,3</sup>

<sup>1</sup> School of Resources and Civil Engineering, Northeastern University, Shenyang 110819, China; qxyysy@163.com (X.Q.)

<sup>2</sup> Institute of Resource Utilization and Rare Earth Development, Guangdong Academy of Sciences, Guangzhou 510651, China

<sup>3</sup> State Key Laboratory of Separation and Comprehensive Utilization of Rare Metal, Guangzhou 510651, China

\* Correspondence: 1910374@stu.neu.edu.cn

**Abstract:** The high reactivity of the acetylene group enables the formation of strong chemical bonds with active sites on mineral surfaces, thereby improving the flotation performance of gold minerals. This study utilized density functional theory (DFT) to analyze the quantum chemical parameters of structure, Mulliken population, and the frontier orbitals of a thioester collector containing an acetylene group, PDEC (prop-2-yn-1-yl diethylcarbamodithioate). PDEC was compared with analogous thioester collectors Z-200 and Al-DEC DT. The interaction mechanism of PDEC on the Au(1 1 1) surface was simulated, followed by empirical validation through adsorption experiments. The findings indicate that the S atom of PDEC in the carbon–sulfur group exhibits shorter covalent bond lengths, and has reduced carbon–sulfur double bonds and Mulliken population, resulting in enhanced electron localization. This confers greater selectivity to PDEC during its adsorption on mineral surfaces. Frontier orbital analysis shows that the electrons of the acetylene group possess a notable electron-accepting capacity, significantly influencing the frontier orbital energy of PDEC and playing a pivotal role in the bonding interaction with mineral surfaces. Both the S atom in the carbon–sulfur group and its acetylene group establish stable adsorption structures with the A(111) surface in a single coordination mode. The adsorption energy sequence is PDEC > Al-DEC DT > Z-200. Partial density of states demonstrates that the S 3p orbit of the carbon–sulfur group hybridizes with the Au 5d orbit, while the C 2p orbit of the acetylene group engages in weaker back-donation bonding with the Au 5d orbit. This is corroborated by the electron density difference and post-adsorption Mulliken population analyses, revealing that the S atom of the carbon–sulfur group in PDEC donates electrons to the Au atom, forming dominant positive coordination bonds, whereas the acetylene group accepts partial electrons from the Au atom, resulting in weaker back-donation bonds. The adsorption experiments align with the DFT adsorption energy results.



**Citation:** Qiu, X.; Qi, Y.; Wei, D.; Zhang, F.; Wang, C. Interactions of Acetylene-Derived Thioester Collectors with Gold Surfaces: A First-Principles Study. *Minerals* **2024**, *14*, 238. <https://doi.org/10.3390/min14030238>

Academic Editors: André C. Azevedo and Rafael Teixeira Rodrigues

Received: 17 January 2024

Revised: 23 February 2024

Accepted: 23 February 2024

Published: 26 February 2024



**Copyright:** © 2024 by the authors. Licensee MDPI, Basel, Switzerland. This article is an open access article distributed under the terms and conditions of the Creative Commons Attribution (CC BY) license (<https://creativecommons.org/licenses/by/4.0/>).

## 1. Introduction

Gold predominantly exists in its elemental state, and is typically found in quartz veins, sulfide mineral deposits, and placer deposits [1]. Its economic value and significant role in the industrial and technological sectors are well-recognized [2]. Thorough research into gold extraction and purification techniques not only enhances resource utilization efficiency but also fosters sustainable development in related industries [3]. The primary methods for gold beneficiation include gravity separation, flotation, cyanidation, and pyrometallurgy. Gravity separation is effective for coarse-grain gold ores, while flotation suits fine-grain gold ores. Cyanidation, a chemical extraction method, dissolves gold in cyanide solutions, and pyrometallurgy involves processes such as smelting and electrolysis [4,5].

Flotation is recognized as an efficient technique for the enrichment of gold, and is particularly applicable to fine-grained gold ores or complex ores with low gold content.

The success of this method critically hinges on the judicious selection and application of collectors [6,7]. Recent decades have seen notable advancements in research on gold flotation collectors, including sulfide collectors, amino-acid collectors, and multifunctional composite collectors, all of which demonstrate superior efficacy in enhancing gold recovery and selectivity [8–10]. Liu et al. [11] used density functional theory (DFT) calculations at the B3LYP/6-31+G(d) level in both the vacuum and aqueous phases, predicting that di-isobutyl dithiophosphinate (DIBDTPI) demonstrates superior electron-accepting properties and exhibits remarkable selectivity towards gold. Oluwabunmi et al. [12] discovered that using a pulp density of 200 g/L, adjusting with sodium silicate for 5 min to pH 9.2, and employing 4 g of P-Xanthate along with 0.9 mL of amine glycol, significantly enhanced the gold recovery rate in two-level factorial experiments. In a flotation study conducted by Tan, L. [13] at the Gaowang gold mine, it was found that employing 25 g/t of the thio-urea type collector ZL4020 at a pH of 9.0–9.5 resulted in a gold recovery rate increase of approximately 2% compared to the results for the same dosage of the collector Z200. Beattie et al. [14] employed X-ray photoelectron spectroscopy (XPS) to examine the chemisorbed geometries of 2-mercaptopbenzothiazole (MBT) and di-isoamyl dithiophosphate (DTP) collectors on gold and gold–silver alloy surfaces, in terms of co-adsorption, MBT has a higher affinity for the surface of pure gold, but the addition of silver into the surface layers of the gold substrate swings that balance in favor of DTP. Mineral processing plants predominantly utilize traditional gold collectors like cyanides, which are highly efficient, but pose considerable environmental risks. The method of blending traditional sulfide mineral collectors to treat complex ores with diverse metals or associated minerals is growing more challenging, and the complexity can hinder the effective recovery of gold. Despite notable advancements in the development of novel gold collectors aimed at enhancing gold recovery efficiency, substantial challenges in environmental impact, cost, technological innovation, and sustainability remain to be addressed [15].

Acetylene-based collectors have garnered interest for their high reactivity, enabling strong chemical bonding with sulfides or other reactive sites on mineral surfaces, thereby enhancing mineral flotation performance, particularly in complex ore separation [16]. It was hypothesized that the acetylene group's hydrogen may interact with metals like Cu, Au, and Ag in aqueous solutions, forming organometallic compounds [17]. Burdonov et al. [18] explored a novel collector, 2-methyl-3-butyn-2-ol, which shows promise in augmenting gold recovery from challenging-to-float sulfide minerals through electrostatic adsorption on pyrite surfaces. Yushina, T. I. [19] applied the molecular mechanics (MM2) method to assess the selective fixation of acetylene-containing alcohol collectors, suggesting potential additional gold recovery rates of 2.4% to 5.0% from gold-bearing ores.

Density functional theory (DFT) is a computational quantum mechanics method that involves constructing an effective potential (including the interaction potential between electrons and the external potential), and solving the Kohn-Sham equations to obtain the electron density distribution of the system. From this, the ground state energy of the system and other physical properties, such as the electronic structure, molecular-orbital energy levels, and chemical reactivity, can be calculated [20,21]. Recently, the increasing application of DFT in flotation research has offered fresh insights into the electronic structure of minerals and their flotation behavior. Liu et al. [22] employed DFT to elucidate the molecular interaction mechanism of Diisobutyl Monothiophosphate as a collector in gold pyrite flotation. It revealed that this collector effectively binds to gold mineral surfaces, enhancing gold recovery rates. Yushina et al. [19] investigated the electronic interaction mechanism of unsaturated tertiary alcohol collectors in gold sulfide ore flotation via DFT simulations. The results indicated that these collectors significantly enhance gold flotation selectivity. In conclusion, employing DFT in gold flotation research offers novel insights into the electronic structure of gold minerals and their flotation dynamics. DFT simulations enable researchers to delve into the interaction mechanisms between collectors [23] and gold mineral surfaces, facilitating the design of more efficient and selective flotation collectors [24].

In numerous industrial applications, thioester collectors have been employed to enrich gold. However, the literature lacks reports on the incorporation of acetylene groups into thioester collectors to leverage the unique properties of acetylene groups for improving the flotation efficacy of thioester collectors in gold processing. The motivation of this work is to unveil the mechanism of a thioester collector with an acetylene group, PDEC (prop-2-yn-1-yl diethylcarbamodithioate), on the Au(1 1 1) [25] surface using density functional theory (DFT) calculations [26]. To further this investigation, the highest occupied molecular orbital (HOMO), lowest unoccupied molecular orbital (LUMO) [24], and Fukui function [27] were applied to distinguish and highlight the unique attributes and superiorities of PDEC over other non-ionic thioester collectors. Moreover, the reaction mechanism was meticulously analyzed through the adsorption energy of the collector molecules on the Au surface, the partial density of states (PDOS) [28,29], and the difference density. Subsequently, adsorption experiments on gold powder were performed to corroborate the DFT adsorption energy findings. This article offers guidance on the development of a novel collector for gold, PDEC, and provides new insights into the adsorption principles of acetylene-based collectors on the Au(1 1 1) surface from a quantum chemical perspective.

## 2. Methods

### 2.1. Model and Parameters

The crystal and surface models of gold (Au), along with the molecular and adsorption models of the collectors, were developed using the Visualizer and Amorphous cells tools in Materials Studio 2018. First-principles calculations utilized the CASTEP and Dmol<sup>3</sup> modules [30]. CASTEP was employed for model optimization and adsorption energy, partial density of states (PDOS), and electron density difference calculations. Conversely, Dmol<sup>3</sup> was used for frontier orbital analysis and Fukui function assessments. This approach leverages CASTEP for its proficiency in calculating periodic metal structures and Dmol<sup>3</sup> for its speed in molecular density functional theory calculations. Dmol<sup>3</sup> excels at swiftly optimizing molecular and solid system structures, thereby boosting research productivity. Ultrasoft pseudopotentials facilitated the modeling of interactions between ionic valence and valence electrons.

The Au(1 1 1) surface plays a significant role in surface science and nanotechnology, attributed to its distinctive chemical and physical attributes [31]. As shown in Figure 1, following the optimization of the Au crystal cell, an Au(1 1 1) surface consisting of eight atomic layers was developed. This optimization entailed stabilizing the bottom two layers and permitting the relaxation of the top six atomic layers. Furthermore, a 15 Å vacuum layer was established above the surface.

After evaluating each exchange-correlation function's truncation energy, GGA\_PBESOL demonstrated the closest convergence value to the experimental data, with an error margin of only 1.20%, which falls within the acceptable range. Consequently, GGA\_PBE was selected as the exchange-correlation function. The chosen truncation energy was set at 380 eV, and a k-point grid of  $2 \times 2 \times 1$  was applied for all three surface configurations. Structural optimization was performed using the BFGS algorithm [31], adhering to specific convergence criteria: 0.05 eV/Å for interatomic interaction forces, 0.1 GPa for internal stress,  $2 \times 10^{-3}$  Å for maximum atomic displacement, and  $2 \times 10^{-6}$  eV/atom for self-consistent field accuracy [32].

Two types of thioester collectors, Z-200 (O-isopropyl ethylcarbamothioate) and Al-DECCT (allyl diethylcarbamodithioate), were compared with PDEC (prop-2-yn-1-yl diethylcarbamodithioate). The molecular structure optimization of PDEC, Z-200, and Al-DECCT utilized the same parameters, as illustrated in Figure 2. For Dmol<sup>3</sup> calculations, the Gamma point was employed for k-points, ensuring consistency with the parameters used in CASTEP.

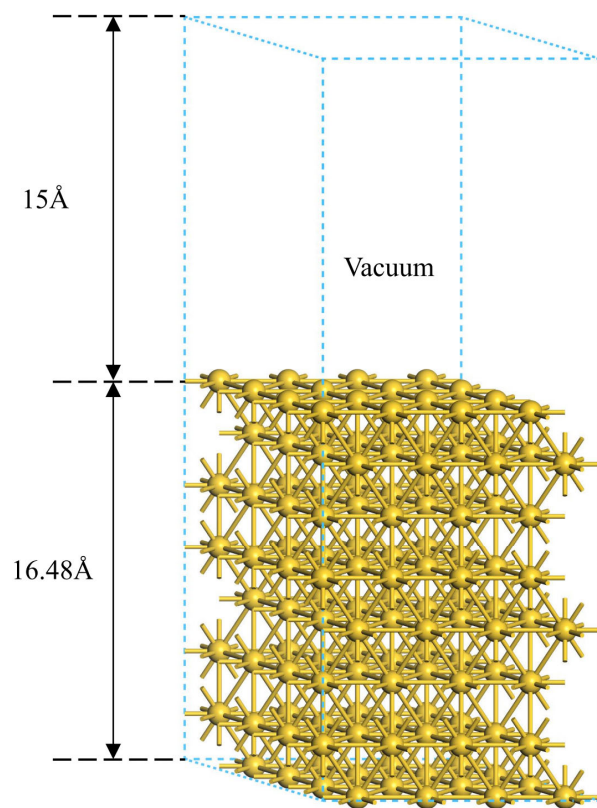


**Figure 1.** Au slab used in the CASTEP calculations (where golden-yellow spheres represent Au atoms).

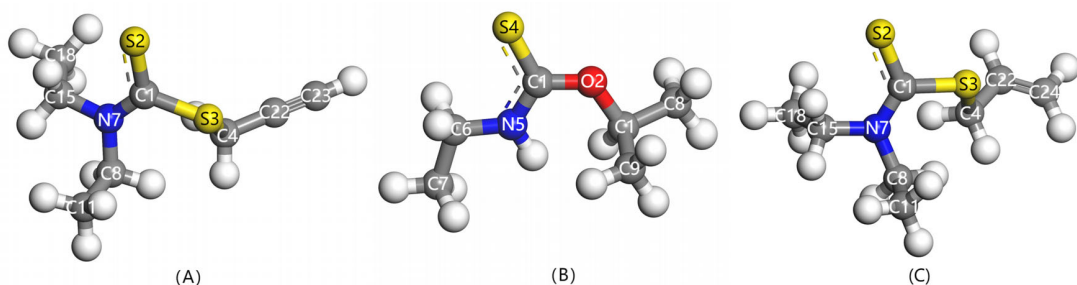


**Figure 2.** Optimized structures of the investigated (A) PDEC, (B) Z-200, and (C) Al-DECDT (where yellow, gray, blue, red, and white spheres represent S, C, N, O, and H atoms, respectively).

## 2.2. Adsorption Energy Calculation

When calculating the surface adsorption energy, electron volts (eV) and kilojoules per mole (kJ/mol) are the prevalent units. This study uses kilojoules per mole (kJ/mol) to articulate energy variations in macroscopic chemical reactions, thereby enhancing the comprehension and analysis of the adsorption process's thermodynamic characteristics [20,21,33–36].

The collector's adsorption energy on the Au surface is calculated using the formula below.  $E_{ad}$  signifies the adsorption energy,  $E_{(Au\text{-surface}+\alpha)}$  the system's total energy post-adsorption,  $E_{Au\text{-surface}}$  the energy of the Au crystal face, and  $E_\alpha$  the energy of the collector. A negative value of  $E_{ad}$  suggests spontaneous adsorption, with a larger absolute value indicating greater ease of adsorption [28,37].

$$E_{ad} = E_{(Au\text{-surface}+\alpha)} - E_{Au\text{-surface}} - E_\alpha \quad (1)$$

Moreover, first-principles calculations are typically conducted under idealized conditions—zero temperature and pressure—neglecting complexities like surface defects. While this approach might introduce discrepancies not associated with experimental outcomes, it simplifies the investigation, aiding researchers in elucidating the essential physical and chemical attributes of materials [20,38,39].

### 2.3. Adsorption Experiments

A  $5 \times 10^{-4}$  mol/L collector solution with 10% ethanol was prepared; this solution was diluted to 100 mL to achieve initial collector concentrations between  $0.6\text{--}1.6 \times 10^{-4}$  mol/L. Concentrations were measured with a UV-Visible spectrophotometer (UV2600, Shunyu Hengping Scientific Instrument Co., Ltd., Shanghai, China) to establish a standard curve. An appropriate volume of ethanol was added during preparation to maintain a uniform 3% ethanol concentration. The solutions, adjusted to pH 9.0 [40–42] with sodium hydroxide solution, were combined with 2 g of gold powder ( $\text{Au} > 99.99\%$ , particle size, 0.074 mm, sourced from Zhongnuo New Material Technology Co., Ltd., Beijing, China) in conical flasks to form a 4% solid concentration gold powder solution. The mixture was stirred magnetically at room temperature for 30 min and then centrifuged at 9000 r/min for 15 min using a TG16-WS machine (Xiangyi Group, Changsha, China). The filtrate's absorbance at its maximum absorption wavelength was recorded, the concentration of residual collector in the filtrate was calculated through interpolation, and the adsorption quantity was calculated by subtraction. The adsorption experiment results represent the mean of three parallel experiments [43–45].

## 3. Results and Discussion

### 3.1. Structure and Mulliken Population

In the CASTEP module of Materials Studio 2018, collectors were analyzed for key bond lengths, compound layouts, and atomic charge distributions, which were optimized, as detailed in Table 1. The S atom in the carbon–sulfur group of the collectors exhibits covalent bond lengths in the order of PDEC > Al-DECDT > Z-200. Shorter bond lengths denote stronger electron localization, indicating a lower propensity for electron loss in the S atom of Z-200 and Al-DECDT compared to that of PDEC. Conversely, the population of carbon–sulfur double bonds in the collectors is in the order of PDEC < Al-DECDT < Z-200, with higher population numbers reflecting stronger covalent bonding. This suggests weaker electron localization in the S atom of Z-200 relative to PDEC and Al-DECDT, aligning with the bond-length findings. Consequently, PDEC exhibits superior selectivity in mineral collection over Al-DECDT and Z-200, based on the carbon–sulfur double bond population. Furthermore, the absolute charge values on the sulfur atoms in the reaction center's carbon–sulfur group of each collector are ranked as follows: Z-200 > Al-DECDT > PDEC. Higher absolute charge values correlate with intensified electrostatic interactions with metal ions on the mineral surface. However, due to the non-directional nature of the electrostatic interactions, stronger interactions do not necessarily enhance the collector selectivity. Thus, in terms of sulfur atom charge, the selectivity ranking of the collectors is PDEC > Al-DECDT > Z-200.

**Table 1.** The magnitude of bond length and the Mulliken population of collectors.

| Collectors | Bond Length (Å) | Mulliken Population of Bond (e) | Mulliken Population of Atom Charge (e) |       |       |       |       |
|------------|-----------------|---------------------------------|--|-------|-------|-------|-------|
|            |                 |                                 | S2                                     | C1    | N7    | S3    | C23   |
| PDEC       | C1-S2           | C1-S2                           | S2                                     | C1    | N7    | S3    | C23   |
|            | 1.669           | 0.90                            | -0.14                                  | -0.17 | -0.27 | 0.23  | -0.38 |
| Z-200      | C3-S4           | C3-S4                           | S4                                     | C3    | N5    | O2    |       |
|            | 1.651           | 0.94                            | -0.19                                  | 0.22  | -0.55 | -0.41 |       |
| Al-DECDT   | C1-S2           | C1-S2                           | S2                                     | C1    | N7    | S3    | C24   |
|            | 1.664           | 0.90                            | -0.15                                  | -0.17 | -0.26 | 0.18  | -0.62 |

### 3.2. Frontier Orbital Analysis

Energy calculations for the optimized models of various collectors were conducted using the Dmol<sup>3</sup> module, with the resulting frontier orbital energies detailed in Table 2. In the context of substrates engaged in complex nucleophilic or electrophilic reactions, the proximity of the energy of LUMO+1 to LUMO necessitates an examination of LUMO+1 [46]. Figure 3 illustrates the significant contribution of the acetylene group to the frontier orbital energies of PDEC, particularly to LUMO+1. This underscores the crucial role of the acetylene group in facilitating bond formation between PDEC and the mineral surface. The delocalized nature of the electrons of the acetylene group enables them to accept additional electrons from the metal atoms of the mineral, thereby forming more stable feedback bonds.

**Table 2.** Frontline orbital energy of collectors.

| Collectors | Frontline Orbital Energy (eV) |        |          |
|------------|-------------------------------|--------|----------|
|            | HOMO                          | LUMO   | LUMO + 1 |
| PDEC       | −4.708                        | −2.077 | −0.608   |
| Z-200      | −4.515                        | −0.812 | 0.510    |
| Al-DECDT   | −4.456                        | −1.942 | −0.895   |

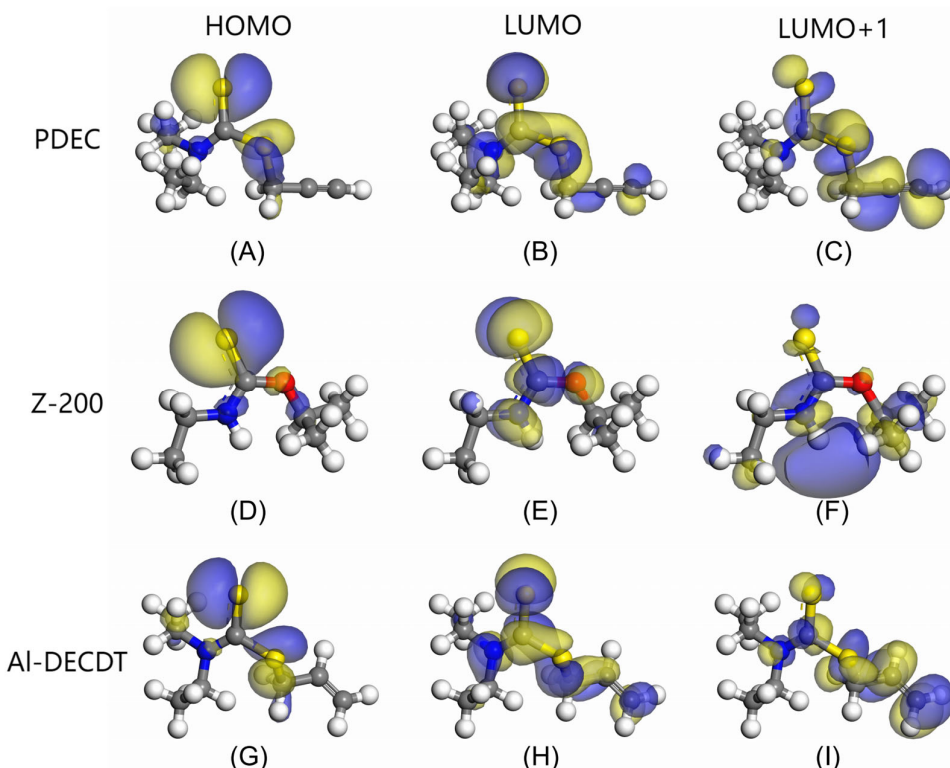


**Figure 3.** HOMO of the (A) PDEC, (D) Z-200, and (G) Al-DECDT clusters; LUMO of the (B) PDEC, (E) Z-200, and (H) Al-DECDT clusters; and LUMO+1 of the (C) PDEC, (F) Z-200, and (I) Al-DECDT clusters (where yellow, gray, blue, red, and white spheres represent S, C, N, O, and H atoms, respectively).

Fukui functions  $f_{w+}$  and  $f_{w-}$ , quantify the propensity for nucleophilic and electrophilic reactions at specific atoms or groups within a molecule. Table 3 demonstrates that, according to Fukui function analysis, the sulfur atoms in the carbon–sulfur groups of the three collectors exhibit the highest  $f_{w+}$  and  $f_{w-}$  values. Notably,  $f_{w-}$  surpasses  $f_{w+}$ , suggesting electron-donating characteristics, which aligns with the HOMO analysis. In comparison, the acetylene group C23 in PDEC ( $f_{w+} = 0.102$ ) shows a greater electron-accepting ability than C24 ( $f_{w+} = 0.065$ ) in the chelating group of Al-DECDT, facilitating nucleophilic interactions between electron-rich metal compounds and electron-deficient acetylene groups.

**Table 3.** Fukui function of collectors.

| Collectors | Atoms | $f_{w+}$ (e) | $f_{w-}$ (e) |
|------------|-------|--------------|--------------|
| PDEC       | S2    | 0.280        | 0.421        |
|            | C1    | 0.079        | 0.017        |
|            | N7    | 0.039        | 0.026        |
|            | S3    | 0.158        | 0.154        |
|            | C23   | 0.102        | 0.081        |
| Z-200      | S4    | 0.365        | 0.572        |
|            | C3    | 0.154        | 0.078        |
|            | N5    | 0.052        | 0.028        |
|            | O2    | 0.064        | 0.013        |
|            | S2    | 0.266        | 0.414        |
| Al-DECDT   | C1    | 0.068        | 0.019        |
|            | N7    | 0.040        | 0.026        |
|            | S3    | 0.138        | 0.161        |
|            | C24   | 0.065        | 0.034        |

### 3.3. Adsorption Energy Comparison

In this work, the carbon–sulfur group serves as the reaction center, with the S atom strategically positioned above an Au atom. To assess the efficacy of the acetylene group in enhancing the adsorption of collectors on the Au(111) surface, accordingly, the acetylene group bond in PDEC and the carbon–carbon double bond in Al-DECDT were aligned parallel to another Au atom. Post-optimization analysis revealed that the most efficient adsorption occurred when the carbon–sulfur double bonds were oriented flat against the crystal surface [47–49], with the S atom directly above the Au atom, yielding the maximum adsorption energy. Figure 4 illustrates the optimal configurations of the collectors on the Au(111) surface, as established through DFT calculations.

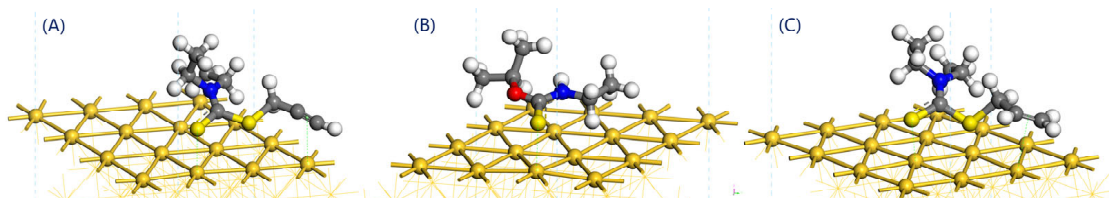


**Figure 4.** Adsorption configuration of (A) PDEC, (B) Z-200, and (C) Al-DECDT on the Au(111) surface, (where golden yellow, yellow, gray, blue, red, and white spheres represent Au, S, C, N, O, and H atoms, respectively).

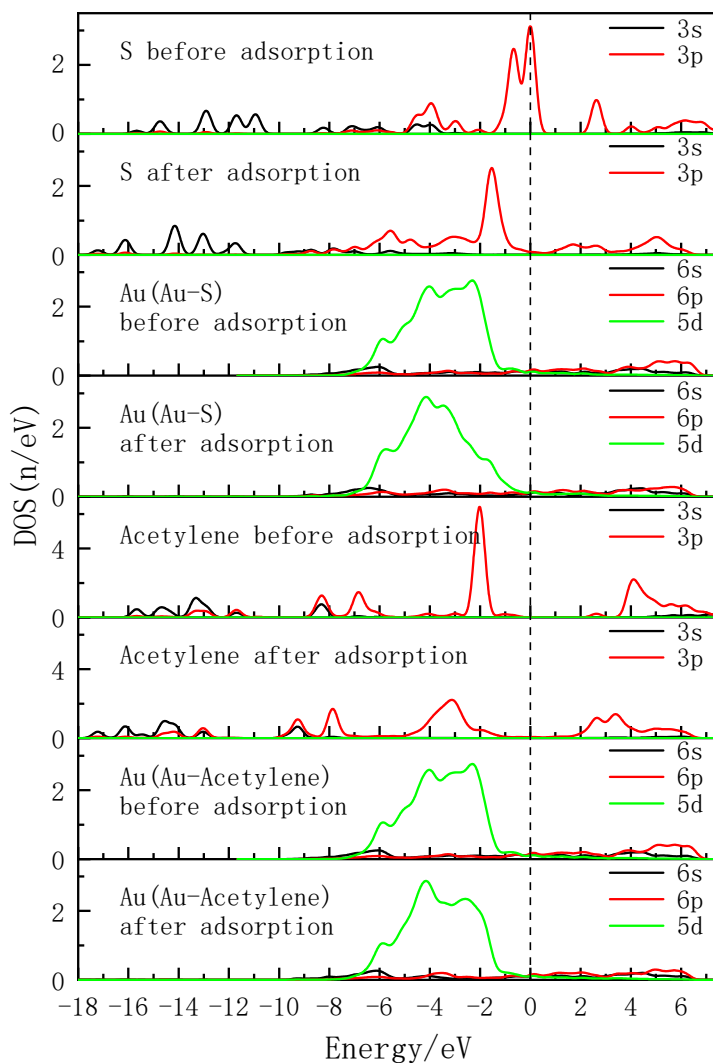
Table 4 delineates the adsorption energy and bond lengths of collectors on the Au(111) surface. The adsorption energy follows the sequence: PDEC > Al-DECDT > Z-200. Post-optimization, the bond lengths of the sulfur atom in the carbon–sulfur group to the Au(111) surface are Z-200 < Al-DECDT < PDEC. However, it is noteworthy that in PDEC, the acetylene group is positioned significantly away from the Au(111) surface, suggesting a likelihood of weak adsorption. Consequently, these findings necessitate an in-depth analysis considering the density of states and electron density difference.

**Table 4.** The adsorption energy calculation and bond length of collectors on Au(111).

| Collectors | Adsorption Energy (kJ/mol) | S-Au Bond Length (Å) |
|------------|----------------------------|----------------------|
| PDEC       | −71.46259119               | 2.580                |
| Z-200      | −58.05373004               | 2.521                |
| Al-DECDT   | −59.43253585               | 2.557                |

### 3.4. Density of States Analysis

PDEC, characterized by its acetylene content, is classified as a non-ionic polar collector. Investigating the interactions between PDEC atomic orbitals and the Au(1 1 1) surface is pivotal in elucidating the chemical interactions between PDEC and gold ore surfaces. Figure 5 illustrates the density of states for the collector both pre- and post-adsorption onto the Au(1 1 1) surface. To delve into the interaction dynamics of PDEC with the Au(1 1 1) surface, a comparative study was conducted, focusing on the variations in the density of states of the S atom within the carbon–sulfur group, and the terminal hydrocarbon group of the polar moiety (specifically, the acetylene group in PDEC and the olefin group in Al-DEC DT) during the adsorption process.



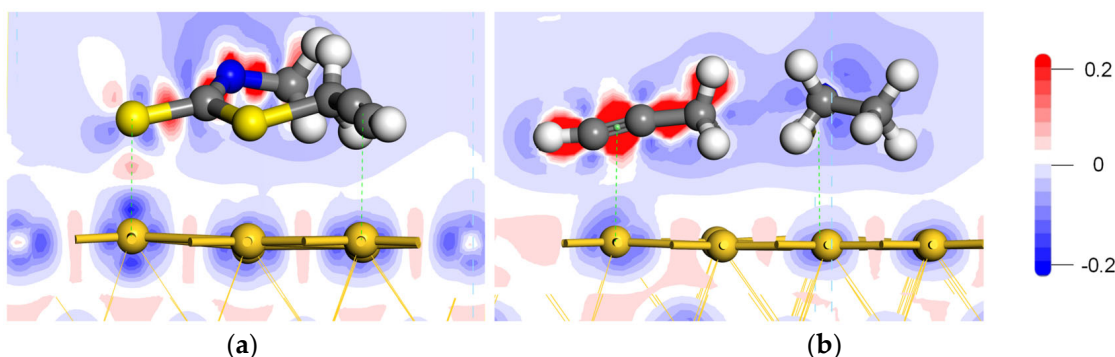
**Figure 5.** Density of states between PDEC on the Au(1 1 1) surface before and after interaction.

Figure 5 delineates the density of states of the sulfur atoms, the acetylene group, and the corresponding gold atoms on surface of Au(1 1 1) in PDEC. At the Fermi level, the energy is normalized to zero, with the DOS spectrum spanning from  $-18$  to  $8$  eV. This region primarily encompasses the bonding and antibonding states of S 3p, C 2p, and Au 5d orbitals. Within PDEC, the 3p orbit of S in the carbon–sulfur double bond traverses the Fermi level. Initially, this 3p state is highly localized; however, post-adsorption, there is a notable shift in the density of the states of S toward lower energy levels. This shift signifies electron loss and an increase in sulfur’s oxidative capacity. Concurrently, there is a reduction in the non-locality of the bonded Au atom’s 5d orbit. Notably, the S 3p and Au 5d orbit

hybridize at  $-2$  to  $-1$  eV and  $-8$  to  $-7$  eV, suggesting robust interactions between S and Au atoms, with sulfur-donating electrons to form a positive bond with gold. Similarly, the contribution of acetylene, primarily from the C 2p orbit near the Fermi level, exhibits a marked localization at  $-2$  eV before adsorption. Following adsorption, the density of states of the acetylene group shifts toward lower energy levels, accompanied by a pronounced reduction in the density peak and the increased non-locality of the C 2p orbit. This trend is also mirrored by the density of states of the Au atom, which shifts modestly toward lower energies. Hybridization between the C 2p and Au 5d orbits at  $-2$  to  $-1$  eV and  $-8$  to  $-6$  eV indicates a weaker feedback bond formation between the acetylene group and the Au atom.

### 3.5. Electron Density Difference

Figure 6a,b illustrate the local electron differential density of the S atom in PDEC's carbon–sulfur group and the acetylene group on the Au(1 1 1) surface. Red and blue denote electron enrichment and depletion, respectively. The contour levels depicted range from  $0.2$  (red) to  $-0.2$  (blue)  $e/\text{\AA}^3$ , where deeper colors signify greater electron enrichment or depletion. In the carbon–sulfur group, the S atom loses electrons to the corresponding Au atom, leading to electron concentration between them, indicative of a strong interaction. Conversely, the C atom at the ends of the acetylene group loses electrons, enriching the electrons on the triple bond, while the corresponding Au atom also loses electrons and overlaps with acetylene. Notably, the Au atom associated with the acetylene group loses fewer electrons than the S atom, implying a weaker interaction with the acetylene group.



**Figure 6.** Electron density difference of PDEC adsorbed on the Au(1 1 1) surface, (a) electron density difference of the S atom in PDEC's carbon–sulfur group on the Au(1 1 1) surface; (b) electron differential density of PDEC's acetylene group on the Au(1 1 1) surface.

Table 5 offers the detailed atomic Mulliken charge populations, elucidating the electron transfer dynamics. Upon the adsorption of PDEC onto the Au(1 1 1) surface, the Au atom linked to the S atom in the carbon–sulfur group exhibits a minor electron loss in the 6s and 5d orbitals, whereas their 6p orbital gains a substantial number of electrons, supplied by the S 3p orbital. The 3p orbital of the C atom in the acetylene group receives some electrons from the corresponding Au atom, forming a back-donation bond.

**Table 5.** Mulliken populations of PDEC atom and Au(1 1 1) atom before and after PDEC adsorbed on the Au(1 1 1) surface.

| Atomic Label | Adsorption Status | s    | p    | d    | Charge (e) |
|--------------|-------------------|------|------|------|------------|
| S            | Before adsorption | 1.83 | 4.31 | 0.00 | -0.14      |
|              | After adsorption  | 1.83 | 4.17 | 0.00 | 0.00       |
| Au(Au-S)     | Before adsorption | 0.91 | 0.53 | 9.65 | -0.09      |
|              | After adsorption  | 0.85 | 0.72 | 9.62 | -0.18      |
| C            | Before adsorption | 1.15 | 3.23 | 0.00 | -0.38      |
|              | After adsorption  | 1.17 | 3.19 | 0.00 | -0.36      |
| Au(Au-C)     | Before adsorption | 0.91 | 0.53 | 9.65 | -0.09      |
|              | After adsorption  | 0.83 | 0.46 | 9.63 | 0.08       |

The findings from the electron differential density and Mulliken charge populations align with the state density analysis. The S atom in PDEC's carbon–sulfur group donates electrons to the Au atom, creating a strong positive coordination bond. Meanwhile, the acetylene group receives some electrons from the Au atom, resulting in a comparatively weaker back-donation bonding, with the positive coordination bonds being predominant.

### 3.6. Adsorption Experiments

Samples of 50 mL each of PDEC, Z-200, and Al-DECDT solutions at various concentrations were prepared. Following the interaction between these collector solutions and the gold powder, their absorbance was measured at their respective maximum absorption wavelengths—252 nm, 246 nm, and 258 nm—using a UV-Visible spectrophotometer. This procedure aimed to determine the quantity of each collector adsorbed onto the gold powder's surface. Figure 7 illustrates the correlation between the adsorption amount and the initial concentration of the collectors. It was noted that the adsorption amount on the gold powder surface proportionally increased with the initial concentration of the collectors. The sequence of adsorption efficiency on the gold powder surface was observed as PDEC > Al-DECDT > Z-200, suggesting that PDEC possesses the most potent collecting capability for gold powder.

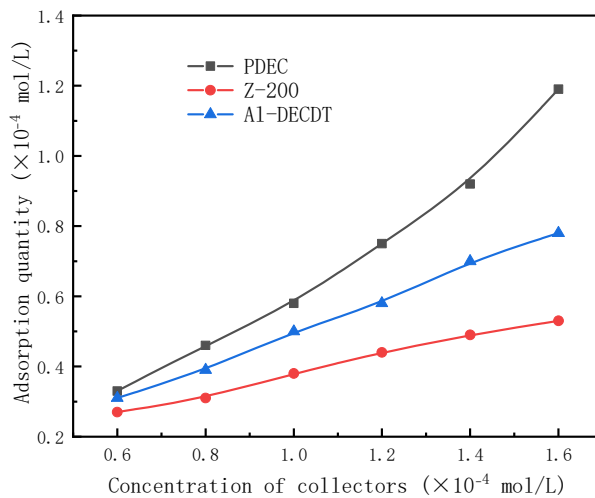


**Figure 7.** Adsorption quantity of PDEC, Z-200, and Al-DECDT on gold powder surfaces as a function of concentration.

## 4. Conclusions

In PDEC, the carbon–sulfur group forms covalent bonds characterized by shorter bond lengths, the reduced carbon–sulfur double bonds and the lower Mulliken population

of the S atom led to enhanced electron localization. This attribute grants PDEC superior selectivity during its adsorption on mineral surfaces.

Analysis of the LUMO+1 orbit indicates that the electrons in the acetylene group of PDEC are delocalized, significantly contributing to the molecule's frontier orbital energy. The C atom in this group ( $f_{w+} = 0.102$ ) demonstrates a robust electron-accepting capacity, underscoring the crucial role of the acetylene group in facilitating bonding interactions with mineral surfaces, particularly in accepting electrons from mineral metal atoms to form stable back-donation bonds.

Both the S atom in the carbon–sulfur group and the acetylene group of PDEC establish stable adsorption structures with the Au(1 1 1) surface, adopting a single coordination mode. The adsorption energy decreases as follows: PDEC > Al-DECDT > Z-200. A partial density of states analysis shows that PDEC's S 3p orbit hybridizes with the Au 5d orbit, forming robust coordination bonds. Conversely, the C 2p orbit in the acetylene group engages in weaker back-donation bonding with the Au 5d orbit. This is further corroborated by the electron density difference and post-adsorption Mulliken population, which confirm the electron donation by PDEC's S atom to the Au atom, while the acetylene group predominantly accepts electrons, with positive coordination bonds being the primary interaction in the adsorption process.

In adsorption experiments, the adsorption quantity of collectors adsorbed onto gold powder surfaces was quantified using a UV-Visible spectrophotometer. The adsorption quantity was observed to increase proportionally with the initial concentration, following the order: PDEC > Al-DECDT > Z-200. These experimental outcomes align with the DFT adsorption energy results.

This work only employed density functional theory (DFT) under ideal conditions and compact adsorption experiments to investigate the mechanism of PDEC on gold surfaces. Future work will focus on incorporating thermodynamic adjustments and accounting for surface heterogeneity to enhance the accuracy of the first-principles calculations, thereby more precisely simulating the adsorption process under real-world conditions. Furthermore, the efficacy of the PDEC collector in flotation will be assessed using authentic ore samples.

**Author Contributions:** Conceptualization, X.Q.; Methodology, Y.Q.; Software, Y.Q.; Validation, F.Z. and C.W.; Formal analysis, Y.Q. and F.Z.; Investigation, Y.Q.; Resources, X.Q. and C.W.; Data curation, Y.Q.; Writing—original draft, X.Q. and Y.Q.; Writing—review & editing, D.W. and C.W.; Supervision, X.Q. and D.W.; Project administration, X.Q.; Funding acquisition, X.Q. All authors have read and agreed to the published version of the manuscript.

**Funding:** This research was funded by Open Project of Yunnan Precious Metals Laboratory Co., Ltd. (YPML-2023050277) and the APC was funded by Institute of Resource Utilization and Rare Earth Development, Guangdong Academy of Sciences.

**Data Availability Statement:** The data that supports the findings of this study is available on request from Yuechao Qi, Northeastern University, upon reasonable request.

**Conflicts of Interest:** Xianyang Qiu and Chenghang Wang received Open Project of Yunnan Precious Metals Laboratory Co., Ltd. (YPML-2023050277) support from Yunnan Precious Metals Laboratory Co., Ltd. The funding sponsors had no role in the design of the study; in the collection, analyses, or interpretation of data; in the writing of the manuscript, and in the decision to publish the results.

## References

- Wu, J.; Ahn, J.; Lee, J. Gold deportment and leaching study from a pressure oxidation residue of chalcopyrite concentrate. *Hydrometallurgy* **2021**, *201*, 105583. [[CrossRef](#)]
- Yang, H.Y.; Wang, S.H.; Song, X.L.; Pan, H.D. Gold occurrence of Jiaojia gold mine in Shandong province. *Trans. Nonferrous Met. Soc. China* **2011**, *21*, 2072–2077. [[CrossRef](#)]
- Arif, J.; Baker, T. Gold paragenesis and chemistry at Batu Hijau, Indoneisa: Implications for gold-rich porphyry copper deposits. *Miner. Depos.* **2004**, *39*, 523–535. [[CrossRef](#)]
- Asamoah, R.K. Specific refractory gold flotation and bio-oxidation products: Research overview. *Minerals* **2021**, *11*, 93. [[CrossRef](#)]

5. Tagirov, B.R.; Filimonova, O.N.; Trigub, A.L.; Vikentyev, I.V.; Kovalchuk, E.V.; Nickolsky, M.S.; Chareev, D.A. The state of gold in phases of the Cu-Fe-S system: In situ X-ray absorption spectroscopy study. *Geosci. Front.* **2023**, *14*, 101533. [[CrossRef](#)]
6. El-Sayed, S.; El-Shatoury, E.H.; Abdel-Khalek, N.A.; Abdel-Motelib, A.; Abdel-Khalek, M.A. Influence of *Bacillus cereus*-gold interaction on bio-flotation of gold in the presence of potassium butyl xanthate. *Biointerface Res. Appl. Chem.* **2021**, *11*, 13005–13018.
7. Wang, S.; Zhang, L.; Lu, D.; Fu, Y. Identification of abnormal conditions for gold flotation process based on multivariate information fusion and double-channel convolutional neural network. *Can. J. Chem. Eng.* **2023**, *101*, 4523–4538. [[CrossRef](#)]
8. Akop, C. Developing a Bulk Circuit Suitable for Chalcopyrite-Pyrite Ores with Elevated Pyrite Content in Copper-Gold Ore Treatment. Master’s Thesis, Sustainable Minerals Institute, The University of Queensland, Brisbane, QLD, Australia, 2014.
9. Bas, A.D.; Larachi, F. The effect of flotation collectors on the electrochemical dissolution of gold during cyanidation. *Miner. Eng.* **2019**, *130*, 48–56. [[CrossRef](#)]
10. Matveeva, T.N.; Gromova, N.K.; Lantsova, L.B. Experimental Proof of Applicability of Cyclic and Aliphatic Dithiocarbamate Collectors in Gold-Bearing Sulphide Recovery from Complex Ore. *J. Min. Sci.* **2021**, *57*, 123–130. [[CrossRef](#)]
11. Liu, G.; Yang, X.; Zhong, H. Molecular design of flotation collectors: A recent progress. *Adv. Colloid Interface Sci.* **2017**, *246*, 181–195. [[CrossRef](#)] [[PubMed](#)]
12. Oluwabunmi, K.E.; Adeleke, A.A.; Adetunji, A.R.; Jeje, S.O.; Abioye, A.A.; Adesina, O.A.; Ibitoye, F.P. 2 k Factorial Experiments on Factors that Influence the Recovery of Gold during the Upgrade of Ilesha-Itagunmodi Gold Ore through Froth Flotation. *J. Miner. Mater. Charact. Eng.* **2014**, *2*, 32–39.
13. Tan, L.; Lin, Q.; Liu, P.; Fu, L. Studies on the flotation separation of a new thionocarbamate—ZL 4020. *Min. Metall. Eng.* **1996**, *16*, 26–29.
14. Beattie, D.A.; Kempson, I.M.; Fan, L.J.; Skinner, W.M. Synchrotron XPS studies of collector adsorption and co-adsorption on gold and gold: Silver alloy surfaces. *Int. J. Miner. Process.* **2009**, *92*, 162–168. [[CrossRef](#)]
15. Zhu, Y.M. Progress in Flotation Reagents Research in 2023. Nonferrous Metals (Mineral Processing Section); 2024, 1–43. Available online: <http://118.89.52.29:8085/kcms/detail/11.1840.TF.20240131.1409.002.html> (accessed on 23 February 2024).
16. Ha, C.S.; Nagappan, S. *Hydrophobic and Superhydrophobic Organic-Inorganic Nano-Hybrids*; CRC Press: Boca Raton, FL, USA, 2018.
17. Nosálová, L.; Maliničová, L.; Kisková, J.; Timková, I.; Sedláková-Kaduková, J.; Pristaš, P. Cultivable microbiota associated with gold ore from the rozália gold mine, hodruša-hámre, Slovakia. *Geomicrobiol. J.* **2021**, *38*, 415–425. [[CrossRef](#)]
18. Burdonov, A.; Vchislo, N.; Barakhtenko, V.; Sahabutdinova, T. Synthesized collectors flotation activity study based on fluorine containing and acetylene alcohols. *Sustain. Dev. Mt. Territ.* **2023**, *15*, 707–719. [[CrossRef](#)]
19. Yushina, T.I. Justification of applying collectors from the class of unsaturated tertiary alcohols in flotation of gold-bearing sulphide ores. *Non-ferrous Met.* **2022**, *2022*, 3–10. [[CrossRef](#)]
20. Merrill, M.D. First principles of instruction. *Educ. Technol. Res. Dev.* **2002**, *50*, 43–59. [[CrossRef](#)]
21. Freysoldt, C.; Grabowski, B.; Hickel, T.; Neugebauer, J.; Kresse, G.; Janotti, A.; Van de Walle, C.G. First-principles calculations for point defects in solids. *Rev. Mod. Phys.* **2014**, *86*, 253. [[CrossRef](#)]
22. Liu, W.; Miller, J.D.; Sun, W.; Hu, Y. Analysis of the selective flotation of elemental gold from pyrite using diisobutyl monothiophosphate. *Minerals* **2022**, *12*, 1310. [[CrossRef](#)]
23. Dong, Z.; Jiang, T.; Xu, B.; Zhong, H.; Zhang, B.; Liu, G.; Yang, Y. Density functional theory study on electronic structure of tetrahedrite and effect of natural impurities on its flotation property. *Miner. Eng.* **2021**, *169*, 106980. [[CrossRef](#)]
24. Mkhonto, P.P.; Chauke, H.R.; Ngoepe, P.E. The effect of thiol collectors on nickel-rich (110) pentlandite surface using density functional theory. In Proceedings of the SAIP2017, the 62nd Annual Conference of the South African Institute of Physics, Stellenbosch, South Africa, 3–7 July 2017; pp. 95–100.
25. Yuan, M.; Feng, X.; Yan, T.H.; Chen, J.; Ma, X.; Cunha, P.; Wang, Y. Superparamagnetic iron oxide-enclosed hollow gold nanostructure with tunable surface plasmon resonances to promote near-infrared photothermal conversion. *Adv. Compos. Hybrid Mater.* **2022**, *5*, 2387–2398. [[CrossRef](#)]
26. Nenchev, G.; Diaconescu, B.; Hagelberg, F.; Pohl, K. Self-assembly of methanethiol on the reconstructed Au (111) surface. *Phys. Rev. B* **2009**, *80*, 081401. [[CrossRef](#)]
27. He, J.; Sun, W.; Chen, D.; Gao, Z.; Zhang, C. Interface interaction of benzohydroxamic acid with lead ions on oxide mineral surfaces: A coordination mechanism study. *Langmuir* **2021**, *37*, 3490–3499. [[CrossRef](#)]
28. He, Y.; Wang, Z.; Ren, Z.; Zheng, R.; Gao, H.; Chen, Z. The Influence of Surface Heterogeneity of Fluorite on the Adsorption of Alkyl Sulfonates. *Minerals* **2023**, *13*, 1005. [[CrossRef](#)]
29. Xu, B.; Wu, J.; Dong, Z.; Tao, J.; Qian, L.; Yang, Y. Flotation performance, structure–activity relationship and adsorption mechanism of a newly-synthesized collector for copper sulfide minerals in Gacun polymetallic ore. *Appl. Surf. Sci.* **2021**, *551*, 149420. [[CrossRef](#)]
30. Cao, S.; Cao, Y.; Liao, Y.; Ma, Z. Depression mechanism of strontium ions in bastnaesite flotation with salicylhydroxamic acid as collector. *Minerals* **2018**, *8*, 66. [[CrossRef](#)]
31. Corso, M.; Fernández, L.; Schiller, F.; Ortega, J.E. Au (111)-based nanotemplates by Gd alloying. *ACS Nano* **2010**, *4*, 1603–1611. [[CrossRef](#)] [[PubMed](#)]
32. Li, M.; Sun, B.; Ao, Z.; An, T.; Wang, G. Atomic-scale identification of influencing factors of sodium dendrite growth on different current collectors. *J. Mater. Chem. A* **2020**, *8*, 10199–10205. [[CrossRef](#)]

33. Loffreda, D. Theoretical insight of adsorption thermodynamics of multifunctional molecules on metal surfaces. *Surf. Sci.* **2006**, *600*, 2103–2112. [[CrossRef](#)]
34. Sergiievskyi, V.P.; Jeanmairet, G.; Levesque, M.; Borgis, D. Fast computation of solvation free energies with molecular density functional theory: Thermodynamic-ensemble partial molar volume corrections. *J. Phys. Chem. Lett.* **2014**, *5*, 1935–1942. [[CrossRef](#)] [[PubMed](#)]
35. Amsler, J.; Plessow, P.N.; Studt, F.; Bucko, T. Anharmonic correction to adsorption free energy from DFT-based MD using thermodynamic integration. *J. Chem. Theory Comput.* **2021**, *17*, 1155–1169. [[CrossRef](#)] [[PubMed](#)]
36. Ren, Z.; Shen, Y.; Gao, H.; Chen, H.; Liu, C.; Chen, Z. Comparison of Sodium Oleate and Sodium Petroleum Sulfonate for Low-Temperature Flotation of Fluorite and the Collecting Mechanisms. *Min. Met. Explor.* **2021**, *38*, 2527–2536. [[CrossRef](#)]
37. Baldridge, K.; Klamt, A. First principles implementation of solvent effects without outlying charge error. *J. Chem. Phys.* **1997**, *106*, 6622–6633. [[CrossRef](#)]
38. Sure, R.; Brandenburg, J.G.; Grimme, S. Small atomic orbital basis set first-principles quantum chemical methods for large molecular and periodic systems: A critical analysis of error sources. *ChemistryOpen* **2016**, *5*, 94–109. [[CrossRef](#)] [[PubMed](#)]
39. Mishra, S.; Panda, S.; Akcil, A.; Dembele, S. Biotechnological avenues in mineral processing: Fundamentals, applications and advances in bioleaching and bio-beneficiation. *Miner. Process. Extr. Metall. Rev.* **2023**, *44*, 22–51. [[CrossRef](#)]
40. Nie, Y.M.; Liu, S.X.; Dai, Q.H. Rough Flotation Research of Low Grade Gold Ore. *Appl. Mech. Mater.* **2014**, *543*, 3822–3825. [[CrossRef](#)]
41. Janštová, S.; Janáková, I.; Čablík, V. Leaching of Gold from Fine-grained Flotation Tailings. *GeoScience Eng.* **2020**, *66*, 117–120. [[CrossRef](#)]
42. Toktar, G.; Bakrayeva, A.; Abdyldayev, N.; Banks, G.E.; Kubaizhanov, A. Increase in the Free Finely-Dispersed Gold Recovery in the Flotation Cycle. *J. Ecol. Eng.* **2023**, *24*, 115–119. [[CrossRef](#)]
43. Zhang, H.Q.; Wang, F.L. Adsorption Selectivity of Fatty Acid Collector by Synthetic Magnetite. *Appl. Mech. Mater.* **2014**, *552*, 263–268. [[CrossRef](#)]
44. Smart, R.S.; Amarantidis, J.; Skinner, W.M.; Prestidge, C.A.; La Vanier, L.; Grano, S.R. *Surface Analytical Studies of Oxidation and Collector Adsorption in Sulfide Mineral Flotation*; Springer: Berlin/Heidelberg, Germany, 2003; pp. 3–62.
45. Ge, Y.Y.; Huang, L.; Xiong, X.H.; Yu, Y.F. Mechanism of a new collector alkyl polyamine ether adsorption on jasper and magnetite. *J. Cent. South Univ. (Sci. Technol.)* **2014**, *45*, 1377–1383.
46. Terzi, M.; Kursun, I.; Cinar, M.; Ozdemir, O. Digital image processing (DIP) application on the evaluation of ironrich heavy mineral concentrates produced from river sand using a sequential mineral processing approach. *Physicochem. Probl. Miner. Process.* **2021**, *57*, 21–35. [[CrossRef](#)]
47. Yang, K.; Lu, X.C.; Liu, X.D.; Hou, Q.F. Characterization technique ii of mineral material based on probe gas adsorption isotherm: Nano-pore structure of porous material. *Bull. Mineral. Petrol. Geochem.* **2006**, *25*, 362–368.
48. Tkatchenko, A.; Scheffler, M. Accurate Molecular Van Der Waals Interactions from Ground-State Electron Density and Free-Atom Reference Data. *J. Phys. Rev. Lett.* **2009**, *102*, 073005. [[CrossRef](#)] [[PubMed](#)]
49. Zierhut, A.; Leopold, K.; Harwardt, L.; Worsfold, P.; Schuster, M. Activated gold surfaces for the direct preconcentration of mercury species from natural waters. *J. Anal. At. Spectrom.* **2009**, *24*, 767–774. [[CrossRef](#)]

**Disclaimer/Publisher’s Note:** The statements, opinions and data contained in all publications are solely those of the individual author(s) and contributor(s) and not of MDPI and/or the editor(s). MDPI and/or the editor(s) disclaim responsibility for any injury to people or property resulting from any ideas, methods, instructions or products referred to in the content.